Next Materials 9 (2025) 100952

Contents lists available at ScienceDirect

Next Materials

journal homepage: www.sciencedirect.com/journal/next-materials

Research article

Alternative source of chitosan for the direct laser synthesis of Ag@chitosan composites with antibacterial and photocatalytic properties

M. Marsico [a], A. Guarnieri [a], M. Triunfo [a], M. Curcio [a], A. Galasso [a], C. Scieuzo [a,b], R. Salvia [a,b], P. Falabella [a,b], R. Teghil [a], A. De Bonis [a,*]

[a] Dipartimento di Scienze di Base e Applicate - DISBA, Università della Basilicata, viale dell'Ateneo Lucano, 10, Potenza 85100, Italy
[b] Spinoff XFlies s.r.l, University of Basilicata, Potenza, Italy

ARTICLE INFO

Keywords:
Chitosan
Silver nanoparticles
Laser ablation in liquid
Hermetia illucens
Antibacterial activity
Photodegradation

ABSTRACT

In this study, we used chitosan obtained from the pupal exuviae of the insect *Hermetia illucens* to produced silver nanoparticles (Ag@CSE) by nanosecond laser ablation in liquid technique. The physic-chemical and functional properties of the obtained nanocomposite were compared to Ag@CS prepared by using a solution of chitosan from crustaceans as liquid, in the same experimental conditions. The composites were studied by transmission electron microscopy (TEM), Uv-vis and FTIR and X-ray photoelectron spectroscopy (XPS) and X-ray diffractometry (XRD). The composites exhibit optical absorption at around 400 nm due to the presence of silver nanoparticles with a diameter of 11 and 14 nm for Ag@CS and Ag@CSE, respectively. We evaluated the antimicrobial capacity of these nanocomposites against two bacterial strains, *Escherichia coli* and *Micrococcus flavus*, by agar diffusion test and microdilution assay. Both composites showed a zone of inhibition of approximately 9 mm against both bacterial strains. Ag@CSE showed marked antimicrobial activity against *E. coli* up to 0.006 g/L, at which value Ag NPs alone lost their activity. The ability to photocatalyse the methylene blue degradation reaction of Ag@CS and Ag@CSE was tested under simulated solar irradiation conditions. The obtained results suggest that chitosan from HE is a valuable alternative source to chitosan from crustaceans and that the obtained composites can be considered for biomedical and photodegradation applications.

1. Introduction

Combining polymers with inorganic nanoparticles represents a strategic approach for developing cutting-edge nanomaterials with multifaceted capabilities that present unique and enhanced properties. Nanometal-polymer composites (NPCs) stand out as a noteworthy and contemporary field of scientific exploration [1,2]. This is due to their ability to integrate metallic nanoparticles with diverse functionalities within a polymer matrix. This integration enriches the polymer with novel and distinctive properties that were previously unattainable. For instance, the presence of metallic nanoparticles with optoelectronic qualities into the polymer framework can impart traits such as enhanced light absorption, emission, and conductivity [3]. These features are particularly valuable in the development of advanced optoelectronic devices, photovoltaics, and light-emitting materials. Furthermore, by considering metallic nanoparticles with antibacterial properties it is possible to obtain NPCs that can inhibit bacterial growth. This aspect has vital implications in areas like medical devices, antimicrobial coatings, and healthcare textiles [4]. NPCs with catalytic activity find utility in diverse applications including environmental remediation, industrial processes, and renewable energy production. Notably, NPCs have garnered considerable attention as photocatalysts. Their appeal as photocatalytic agents arises from several advantageous attributes, including non-toxicity, lightweight nature, affordability, and the possibility to tailor their optoelectronic and mechanical properties [2].

Among the synthetic strategies proposed for the preparation of nanostructured materials, the Laser Ablation in Liquid (LAL) technique received growing attention thanks to its flexibility and simplicity [5]. In LAL experiments, the interaction of an intense laser beam with a solid target results in the local evaporation of the target and the formation of a laser induced plasma that is confined in the liquid. The nucleation and growth of nanoparticles take place into an oscillating cavitation bubble. At the cavitation bubble collapse, the particles are released in the liquid media [6]. Recently, several researchers have studied the laser ablation

* Corresponding author.
E-mail address: angela.debonis@unibas.it (A. De Bonis).

https://doi.org/10.1016/j.nxmate.2025.100952
Received 25 March 2025; Received in revised form 8 July 2025; Accepted 15 July 2025
Available online 17 July 2025

of metals in solutions of polymers, obtaining composite systems with enhanced functional properties [7–14]. Among natural polymers, chitosan (CS), a biopolymer derived from chitin, exhibits excellent biocompatibility, biodegradability, and low toxicity, making it an attractive candidate for various biomedical, environmental, and industrial applications. With a structure closely resembling that of cellulose, CS exhibits an interesting balance between structural rigidity and chemical reactivity [15]. The limited solubility of CS in water lends its utility as a polymeric photocatalyst/adsorbent for removing organic/inorganic pollutants from wastewater. The carbon chain backbone including NH2 groups and OH groups enables CS to have high affinity toward several transition metal ions, that can be adsorbed by either chelation and/or ion exchange. Moreover, CS can act as a stabilizer during the formation of metal NPs and prevents their aggregation. The role of the CS concentration on the ablation rate and on the morphological properties of tin oxide nanoparticles obtained by the nanosecond laser ablation of tin in CS solutions has been studied by Khumaeni et al. [7]. Recently CS/inorganic NP composites prepared by laser ablation in liquid has been proposed for their enhanced properties. Menazea et al. demonstrated the increased biocompatibility and antibacterial activity of CS/Au/Bi2O3 [8,9], and CS/PVA/Se [10] composites with respect to the polymers suggesting their suitability for biomedical applications. The dielectrical and electrical conductivity properties of CS/PEO/FeOx [11] and CS/PVA/Au [12], respectively, were studied for electrical applications of nanocomposites. Moreover, several studies were devoted to the capability of the metal/CS composite for the catalytic and photocatalytic degradation of organic pollutants in wastewater [13,14].

Nowadays, the largest amount of CS comes from waste of the fishing industry, but, recently several studies were devoted to the extraction and purification of CS from alternative and more economically and ecologically sustainable sources such as insects and fungi [16]. In particular, it has been proved that chitosan derived from Hermetia illucens is a promising alternative to conventional sources [17].

In this study, we used chitosan obtained from the pupal exuviae of the insect *Hermetia illucens* to produced silver nanoparticles (Ag@CSE) by nanosecond laser ablation in liquid technique. The laser synthesis of Ag NPs has been widely studied [18,19], but, for the first time, to the best of our knowledge, it was used an alternative source of the biopolymer to synthesize nanocomposite by LAL technique. We compared the physic-chemical, antibacterial and photocatalytic ability of Ag@CSE to Ag@CS, prepared by using a solution of chitosan from crustaceans as liquid, in the same experimental conditions The antimicrobial activity of the composites were assessed on *Escherichia coli,* as Gram- negative model bacterium, and on *Micrococcus flavus,* as Gram-positive model bacterium. Experiments were conducted both qualitatively, via agar diffusion assay, and quantitatively, via microdilution assay. Furthermore, the photocatalytic ability in the degradation of MB under simulated solar irradiation for all composites were investigated. The antibacterial and photocatalytic activity of the obtained composites validating the effectiveness of the alternative source of chitosan.

2. Materials and methods

As reported in [20], Ag nanoparticles were prepared by laser ablation of a Ag target (Goodfellows) in acetic acid and chitosan solutions. A solution of acetic acid 0.1 % v/v (pH=4.2) was used to dissolve chitosan (100–300 kDa, 70 % deacetylation degree, from Acros) (CS) and chitosan obtained from pupal exuviae of *H. illucens* (35–40 kDa, 90 % deacetylation degree) (CSE), respectively. Chitosan from pupal exuviae of *H. illucens* was provided from Xflies s.r.l (Potenza, Italy). The biopolymer was obtained following the method described in Triunfo et al. [17]. Solutions with chitosan concentration of 1 g/L (CS and CSE) were stirred at a temperature of 35°C for 4 h until the complete dissolution of the polymers. The LAL experiments were performed with an Nd:YAG laser source (Handy-YAG - Quanta System) operating at a wavelength of 532 nm, repetition frequency of 10 Hz, pulse duration 7 ns and pulse energy of 15 mJ. The laser source was focused vertically on the surface of the solid target using a 50 mm focusing lens. The target was placed on the bottom of a Teflon vessel filled with 20 ml of the respective solutions. The concentration of Ag NPs was assessed by considering the mass of the silver target before and after ablation. The ablation experiments last until a concentration of about 8 mg/L of Ag was obtained. In this conditions, a metal/polymer ratio of about 1:100 was obtained. This value is comparable to that reported in literature for the use of silver nanoparticles as antimicrobial agents [21].

A variety of techniques were used to characterize the obtained composites. Optical properties were investigated by Uv-vis spectroscopy by using a Specord 50/PLUS Analytic Jena spectrophotometer and acquiring the spectra in the 200–800 nm wavelength range. The colloidal solutions were dropped onto a silicon substrate to prepare samples for FTIR XPS and XRD analysis. The Jasco 400 instrument was used to acquire the FTIR spectra in the 400–4000 cm^{-1} region, with a resolution of 4 cm^{-1}. The composition of the Ag@CS was studied by X-ray Photoelectron Spectroscopy (XPS) using the PHOIBOS 100-MCDS spectrophotometer (SPECS). The instrument was equipped with a magnesium anode and spectra were acquired using the Fixed Analyzer Transmission (FAT) configuration with a resolution of 10.0 eV. The crystal structure was investigated by using a Siemens D5000 diffractometer, equipped with a CuK α radiation source (λ = 1.540 Å), the spectra were acquired in the 2θ = 5–50 range, with step size 0.040 and time per step of 4 s. Few drops of the colloidal solutions were dropped on holey carbon film coated copper grids (Agar Scientific) to study morphology and size distribution of Ag NPs by Transmission Electron Microscopy (TEM). A G2 FEI TECNAI instrument operating at 200 kV and equipped with a GATAN CCD was used.

2.1. Antimicrobial assays

Ag NPs, Ag@CS and Ag@CSE solutions were tested. In all experiments, CS, CSE, acetic acid and distilled water were also tested as controls. Following the method reported in Guarnieri et al. [22] agar diffusion test was employed to evaluate the antimicrobial activity of the samples on both *E. coli* and *M. flavus* (at the highest concentration). Diameters of the inhibition zones (mm) were measured and used to assess the antimicrobial activity of the samples. Results are reported as the mean ± standard deviations of three independent biological replicates.

The Minimum Inhibitory Concentration (MIC) values of the samples were determined using a microdilution assay, as reported in Guarnieri et al., 2022. All the experiments were conducted by performing serial dilutions of the stock solutions, obtaining the following concentrations: 1, 0.5, 0.25, 0.125, 0.06, 0.03, 0.015, 0.006 and 0.003 g/L. Acetic acid was also tested separately, at the corresponding dilutions (0.1 %, 0.05 %, 0.025 %, 0.0125 %, 0.006 %, 0.003 %, 0.0015 %, 0.0006 % and 0.0003 %). After the treatments, the plates were incubated overnight at 37°C and the absorbance was measured at 600 nm with a spectrophotometer (Thermo Scientific Multiskan Go), to detect the bacterial concentrations. The lowest concentration at which the samples are active is defined as the MIC.

All measurements were performed in three biological replicates. Data were expressed as average ± standard deviation and were analyzed by one-way Anova and Bonferroni *post-hoc* test. Statistical analyses were performed using a GraphPad Prism version 6.0.0 for Windows (GraphPad Software, La Jolla, California USA—www.graphpad.com).

2.2. Photocatalytic activity

Solutions of methylene blue (MB) (Sigma-Aldrich) with concentration ranging from 50 to 6.25 mg/L were prepared by dissolving the analytical grade dye in water. 1 ml of the dye solution was added to 49 ml of the composites solution (polymer 1 g/L; AgNps 8 mg/L) for a

final volume of 50 ml and a MB concentration ranging from 1 to 0.125 mg/L. CS and CSE were tested as control.

Before each irradiation, the solutions were stirred in dark for 30 min in order to reach the adsorption equilibrium condition. The photocatalytic process was activated by exposing the solutions to a Osram Ultra Vitalux lamp (300 W, irradiance of 10.7 mW/cm2), specially designed for sunlight simulation. The lamp was placed at a distance of about 15 cm. The solutions were continuously stirred and all the degradation reactions were conducted in an ice bath at controlled temperature of 10°C to limit the solvent evaporation. The residual dye concentration was measured at controlled time by Uv-vis spectrometer considering the maximum absorption of the MB absorbance at 633 nm. All experiments were performed in three replicates.

3. Results and discussion

A comprehensive characterization of the synthesized composites was conducted by using spectroscopic, microscopic and diffractometric techniques. In order to study the optical properties of the synthesized composites, the Uv-vis absorption spectrum of each sample was measured. The structure of CS lacks conjugated double bonds and the low intensity absorption centered at about 285 nm visible in Fig. 1a, can be related to the electronic n—π* transitions of nitrogen and oxygen in the amino and acetamide groups [19,23]. It can be observed that the intensity of this band increases for the CSE, suggesting a higher amount of these functional groups for this alternative source of chitosan. The formation of Ag NPs by the laser ablation of Ag in CS and CSE solutions is confirmed by the presence of the surface plasmon resonance (SPR) band centered at about 400 nm (Fig. 1b). Colloidal solutions with a metal concentration of 8 μg/ml was obtained both for Ag@CS and Ag@CSE. The absorption intensity of SPR band decreases of about 15 % and less than 30 % during several weeks for the Ag@CS and Ag@CSE, respectively. The higher stability of Ag@CS composite can be related to the higher molecular weight of this polymer with respect to CSE. Considering Ag@CS, the position and FWHM of the SPR band are almost retained over 60 days, suggesting the ability of the polymer to stabilize the Ag NPs and to prevent their oxidation and aggregation over the time (Fig. 1c)

Several TEM images were acquired to characterize the nanoparticles morphology, to evaluate their size and observe the presence of crystalline domains. In Fig. 2a and b the TEM image and the size distribution of AgNPs produced in acetic acid 0.1 % are shown. The size distribution is dominated by the high number of particles with a diameter below 10 nm, but larger particles are visible, also. The mean diameter, evaluated considering more than 150 NPs, is 8.4 nm. Spherical NPs with a mean diameter of 11 nm and 14 nm are visible in TEM images of Ag@CS and Ag@CSE, respectively (Fig. 2c and 2f). Larger nanoparticles are enveloped by a thin light shell (Fig. 2d), confirming the coating of Ag NPs by the polymer. The polycrystalline structure of NPs are clearly visible in Fig. 2g. The evaluated lattice distance of 0.24 nm can be related to the distance of planes (111) of Ag in the fcc crystal structure [24]. It cannot be excluded that the presence of some larger particles (with a diameter of several tens nanometers) can be related to secondary laser effects that are active during the nanoparticles synthesis, such as the re-irradiation of the colloidal solution [25].

FTIR spectra of CS and CSE (Fig. 3a) confirm that the polymer obtained by the pupal exuviae of *H.illucens* present the all vibrational bands typical of chitosan: the broad band between 3600 and 3000cm-1 is the result of the O-H and N-H stretching vibration, the band at about 2800cm-1 is related to the C-H stretching vibrations. The signals at 1670, 1580 and 1315 cm^{-1}, are related to the stretching of C═O bonds in amide II, to the bending of N-H bond of amide II and to the stretching of C-N bond of amide III, respectively [17,26]. All the bands characteristic of the polymer can be observed in the composites, also, confirming that the functional groups of the polymer were preserved during the ablation process. Some differences can be observed in the region of the amide II band (about 1570cm-1), suggesting the interaction of the N-H groups with the metallic NPs. [27].

XRD spectrum of Ag NPs obtained by LAL (Fig. 3c), shows a peak at 38.2° assigned to (111) planes of silver in the FCC structure (JCPDS card no. 87–0720). A dimension of 20 nm for crystalline domains was evaluated by the Scherrer formula. XRD of CS, CSE, Ag@CS and Ag@CSE are shown in Fig. 3b. All XRD spectra are dominated by a broad band centered at about 20°. This band is sharper for CSE than for CS, suggesting the presence of larger crystalline domains in the chitosan obtained from the exuviae of *H.illucens*. The presence of larger crystalline domains is probably related to the higher deacetylation degree for CSE with respect to CS [17]. Low-intensity signals at 9° and 12° in the diffractograms of CSE and Ag@CSE suggest the presence of residual chitin [17]. Silver synthesis in chitosan solutions slightly affects the polymeric crystalline structure, as suggests the broadening of the band centered at 20° for Ag@CS and Ag@CSE samples. The low intensity signal at 38.2° in Ag@CS diffractogram confirms the presence of metal nanoparticles in the composite.

In the XPS spectrum of Ag@CS sample (Fig. 3c) the signals of the polymer (C1s, O1s and N1s at binding energy of 285 eV, 531 eV and 400 eV, respectively) are clearly visible, whereas it was not possible to detect the signal of the Ag contribution. Since XPS is a very surface sensitive technique, this result suggests that the metal nanoparticles are coated by the polymer. High-resolution XPS spectra along with their respective peak deconvolutions are reported as Supplementary Materials.

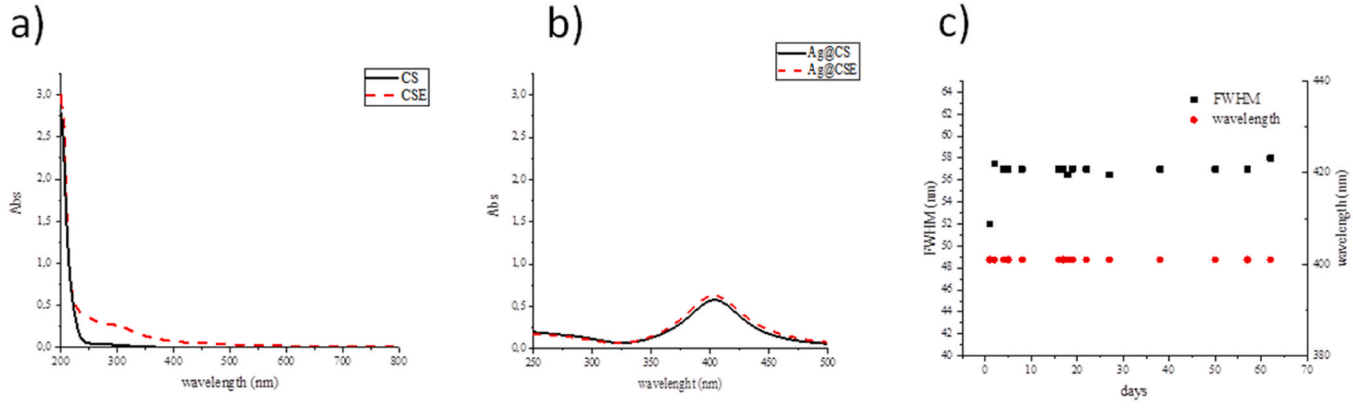

Fig. 1. a) Uv-vis spectra of CS and CSE; b) Uv-vis spectra of Ag@CS (black solid line) and Ag@CSE (red dashed line); c) FWHM and position of the SPR band of Ag@CS over the time.

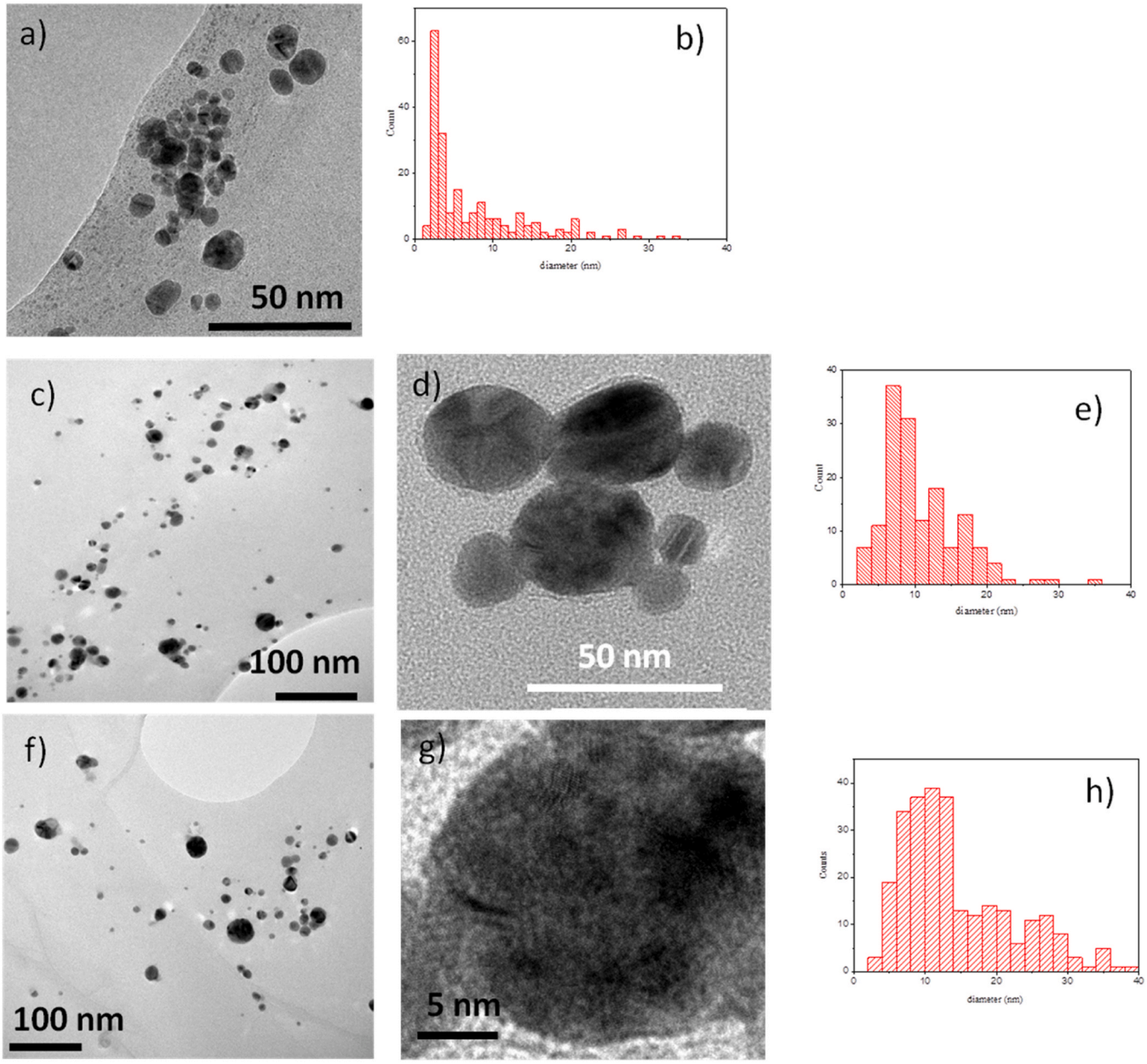

Fig. 2. a): TEM image and b): size distribution of nanoparticles obtained by laser ablation of Ag in acetic acid 0.1 % solution; c, d): TEM image and e): size distribution of nanoparticles in Ag@CS; f, g): and h) size distribution of nanoparticles in Ag@CSE.

4. Antimicrobial activity

Results of the agar diffusion assay performed on *E. coli* and *M. flavus* are reported in Fig. 4.

As reported in Fig. 4, measurable inhibition zones were obtained for all samples tested. Distilled water and acetic acid, as already reported in Guarnieri et al. [22] and Triunfo et al. [28], did not give detectable inhibition zones on either bacteria (Table 2).

On *E. coli*, Ag@CS and Ag@CSE induced the formation of inhibition zones with about 9 mm diameter (Fig. 4; Fig. 4; Table 2). The inhibition zone was larger in diameter for Ag@CSE than for Ag@CS (9 mm vs 8 mm, respectively) (Fig. 5a; Table 1).

The result obtained Ag@CSE was statistically significant compared to all the other diameters obtained. The diameter obtained from Ag@CS was statistically significant compared to the CS solution alone tested. In contrast, no significant differences were obtained between Ag@CSE and Ag@CS. Ag NPs, identified as control, gave no measurable inhibition zones, confirming that the synergy with the biopolymer gives the best inhibitory effect, both for the nanostructures and the solutions as they are. Inhibition zones obtained on *M. flavus* were higher than the results obtained from the same samples on *E. coli,* for all tested samples except CS. Specifically, Ag@CSE resulted in an inhibition zone that was statistically significant compared to Ag@CS; this finding is promising because it implies a greater antimicrobial effect of the nanostructures obtained with insect-chitosan compared to those obtained with the commercial biopolymer, validating the effectiveness of the alternative source. In contrast, Ag@CS resulted in an inhibition zone larger and statistically significant in diameter than CS (Fig. 5b; Table 1). As already demonstrated on Gram-negative bacteria, Ag NPs gave no detectable inhibition zones.

Microdilution assay results for CS, CSE, Ag@CS, Ag@CSE and Ag NPs are shown in Fig. 6. All samples were analysed at nine concentrations: 1, 0.5, 0.25, 0.125, 0.06, 0.03, 0.015, 0.006 and 0.003 g/L.

On *E. coli*, at the highest concentrations, i.e. 1 and 0.5 g/L, Ag@CSE

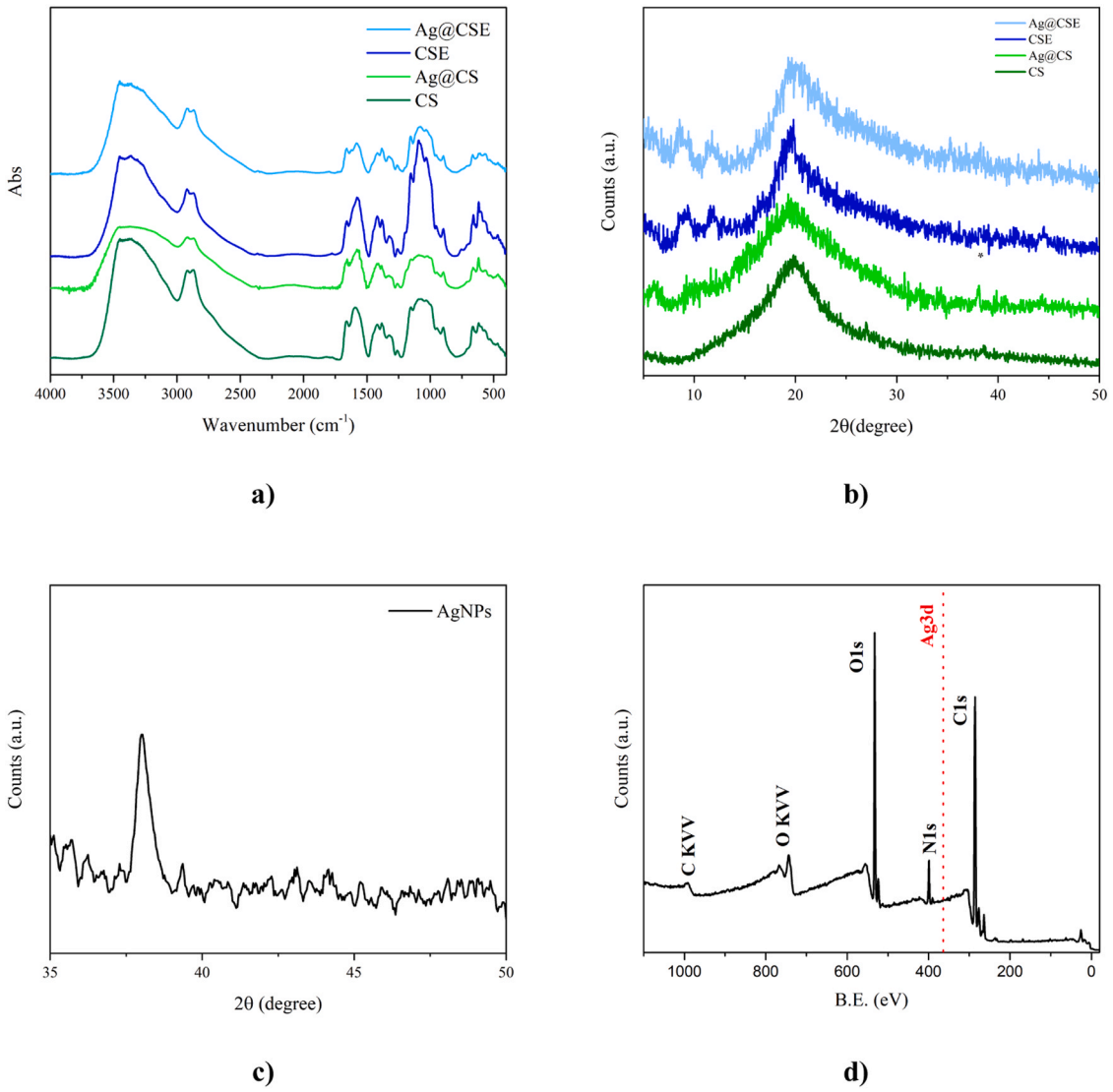

Fig. 3. a) FTIR spectra and b) XRD diffractograms of CS (dark green), Ag@CS (light green). CSE (dark blue) and Ag@CSE (light blue); c) XRD diffractogram of Ag NPs; d) XPS spectrum of Ag@CS. The red dotted line marks the expected position of Ag3d signal.

Table 1
Diameters (mm) of inhibition zones formed by Ag@CSE, Ag@CS, Ag NPs, CSE, CS, acetic acid and distilled water on *E. coli* and *M. flavus*. Distilled water was tested as negative control. Results are expressed as mean ± standard deviation of diameters measured with agar diffusion test of three independent biological replicates. Different letters indicate significant differences ($p < 0.05$) among treatments.

BACTERIAL SPECIES	SAMPLE	Diameter (mm)
E. coli	Ag@CSE	9 ± 0.4^{a}
	Ag@CS	8 ± 0.5^{b}
	Ag NPs	-
	CSE	8 ± 0.2^{bc}
	CS	8.5 ± 0.4^{c}
	Acetic acid	-
	Distilled water	-
M. flavus	Ag@CSE	10 ± 0.4^{a}
	Ag@CS	9 ± 0.5^{b}
	Ag NPs	
	CSE	8.5 ± 0.2^{bc}
	CS	8 ± 0.3^{c}
	Acetic acid	-
	Distilled water	-

resulted in a valuable inhibition effect. At the same concentrations, Ag NPs also showed antimicrobial activity. As in case of chitosan sample in solution, in presence of acetic acid the inhibitory effect cannot be attributed to chitosan alone, since at these concentrations acetic acid also exerts its antibacterial effect. Indeed, as reported in Guarnieri et al. [22], it is of primary importance for these experiments to identify the concentration at which chitosan or chitosan nanostructures express their antimicrobial activity, whereas acetic acid loses it.

As shown in Fig. 6a, from 0.5 g/L up to 0.006 g/L, Ag@CSE had a markable antimicrobial activity that Ag NPs alone lost. Thus, 0.006 g/L is the MIC value of Ag@CSE, whose activity is also more intense than Ag@CS. Also the result obtained from CSE confirms this trend, at the same concentrations.

On the other hand, on *M. flavus* (Fig. 6b), when testing the same samples at the same concentrations, Ag@CSE showed good inhibition but did not give statistically significant results compared to Ag NPs. Indeed, at 1, 0.5 and 0.25 g/L, the inhibitory effect was greater for AgNPs than for nanosystems with chitosan. After that, lowering the concentration from 0.125 to 0.015 g/L, there was no significant difference between Ag@CSE and Ag NPs, whereas the activity of Ag@CS is always lower. Even at 0.006 g/L, the activity of Ag NPs was higher. On the Gram-positive bacterium, therefore, it was not possible to identify a

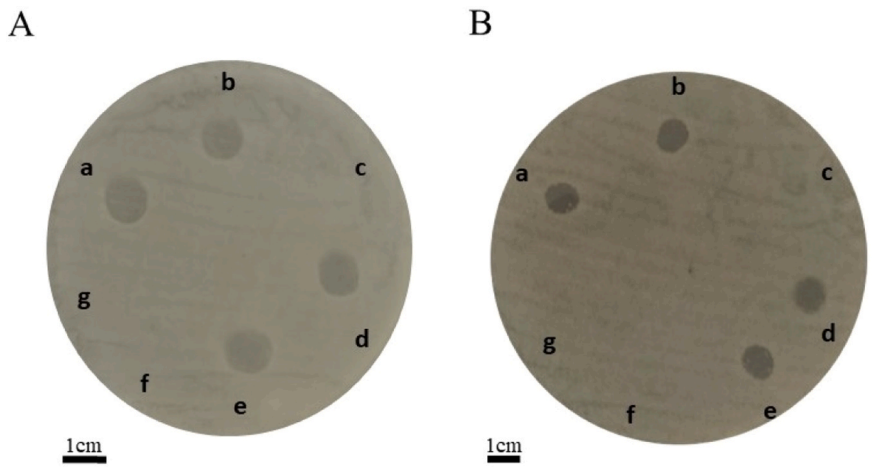

Fig. 4. Inhibition zones of silver sample experiments on *E. coli* (A) and *M. flavus* (B) resulting from the agar diffusion test are reported. Ag@CSE (a), Ag@CS (b), Ag NPs (c), CSE (d), CS (e), acetic acid (f) and distilled water (g).

Table 2
Kinetic constant (k), half time ($t_{1/2}$) and efficiency (η%) for the MB photodegradation reaction at different conditions.

	k(min-1)	$t_{1/2}$ (min)	η%
CS_MB (1 mg/L)	0.0013	533	
CSE_MB (1 mg/L)	0.0015	462	
Ag@CS_MB (1 mg/L)	0.0070	99	40
Ag@CS _MB (0.5 mg/L)	0.0086	80	50
Ag@CS _MB (0.25 mg/L)	0.024	29	85
Ag@CS _MB (0.125 mg/L)	0.098	7	94
Ag@CSE_MB (1 mg/L)	0.0078	89	45

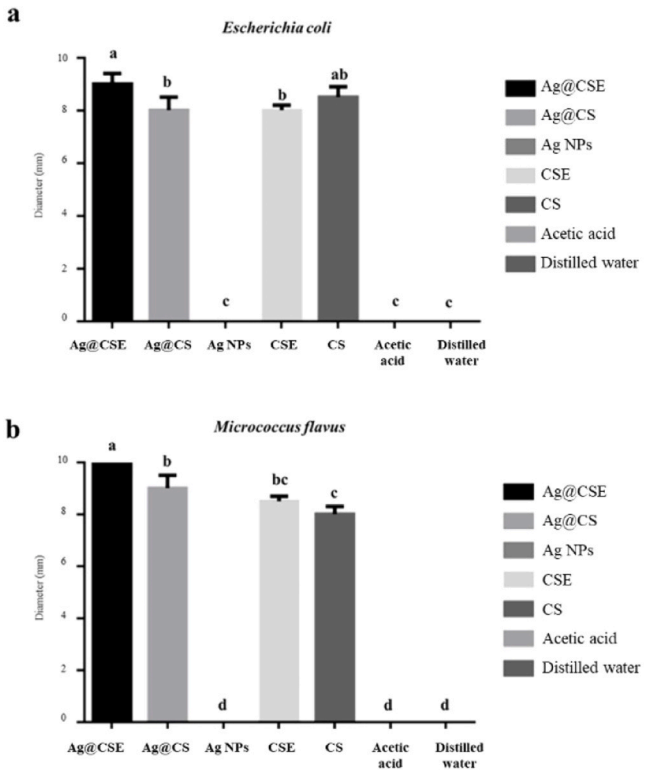

Fig. 5. Graphical representation of silver samples experiments on *E. coli* (a) and *M. flavus* (b) resulting from agar diffusion test. Different letters indicate significant differences ($p < 0.05$) among treatments. Data were analyzed with one-way ANOVA and Bonferroni's *post-hoc* test.

concentration at which the data obtained from the nanoparticles combined with insect-chitosan was statistically significant compared to the Ag NPs. However, the activity of the composite systems is higher with respect to that of polymers for concentration ranging from 0.5 g/L to 0.06 g/L, suggesting that the antibacterial property of silver is retained when the metallic nanoparticles are dispersed in the polymeric network.

4.1. Photocatalytic activity

The catalytic efficiency of the Ag@CS and Ag@CSE composites was investigated by carrying out the photodegradation of MB. The rate constants for the degradation reactions were calculated from the linear least square fitting of the kinetic equation considering a pseudo first order mechanism (Eq.1), whereas, half-time ($t_{1/2}$) and the efficiency of the photodegradation reaction (η) were calculated considering Eqs. (2) and (3), respectively

$$\ln\frac{[C]}{[C_0]} = -k_{app}t \tag{1}$$

$$t_{1/2} = \frac{\ln 2}{k} \tag{2}$$

$$\eta = \left(\frac{C_0 - C}{C_0}\right) * 100 \tag{3}$$

where C_0 is the MB concentration at t = 0 and C is the residual dye concentration. Values of rate constant (k_{app}), half time ($t_{1/2}$) and efficiency for degradation reactions evaluated after 70 min in all the experimental conditions considered are listed in Table 2.

The rate constants for the decoloration of the solution of MB 1 mg/L are 0.0013min-1 and 0.0015min-1 for CS and CSE, respectively, suggesting the adsorption of MB onto the network of the polymer. (Fig. 7). For the reactions of MB photodegradation in Ag@CS and Ag@CSE solutions, a rate constant of 0.0070min-1 and 0.0079min-1 were evaluated for a MB concentration of 1 mg/L, highlighting role of AgNPS in the dye degradation. Considering that the dye concentration plays a relevant role in the degradation kinetics [29], the catalytic capability of Ag@CS was proved at different concentration of MB ranging from 1 to 0.125 mg/L. The kinetic constants increase form 0.007min-1–0.098 min-1 for the higher and lower MB concentration, respectively. The rate constants, efficiency and $t_{1/2}$ for all the experimental conditions are reported in Table3. It can be observed that the photocatalytic efficiency of the composite gradually decreases with the increasing of MB amount. The main reason for this effect can be related to the decrease of the solution transmittance with the increase of the dye concentration

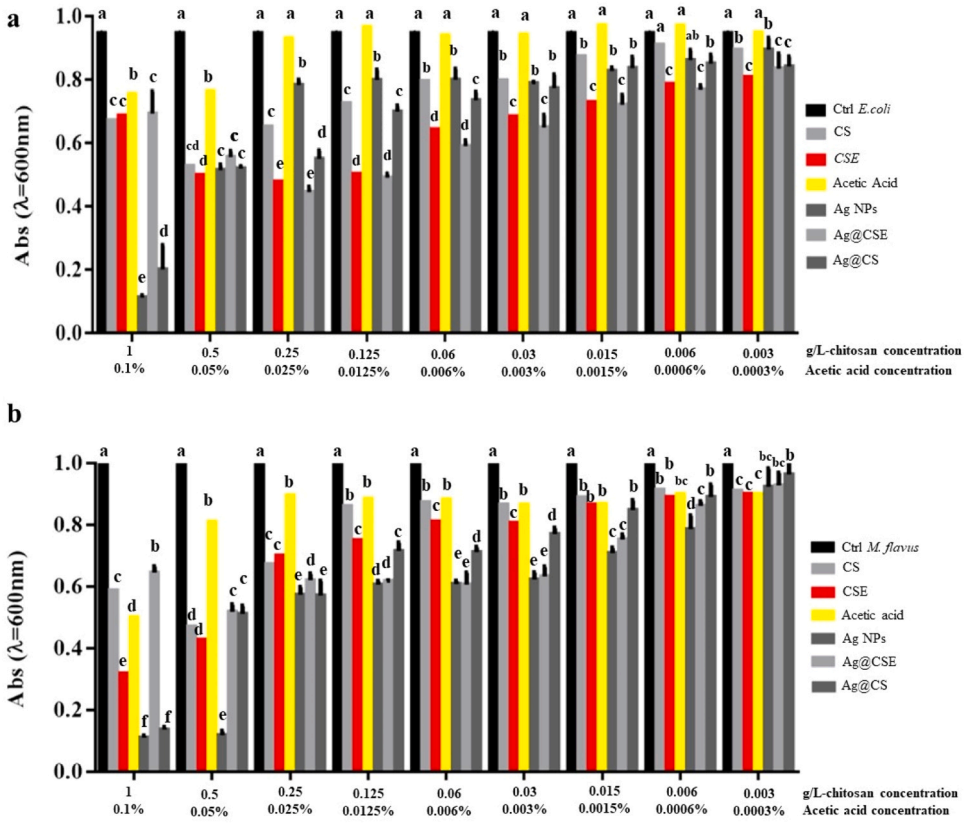

Fig. 6. Results of microdilution assay for Ag@CSE, Ag@CS, Ag NPs, CSE, CS, acetic acid and distilled water at the nine concentrations of 1, 0.5, 0.25, 0.125, 0.06, 0.03, 0.015, 0.006 and 0.003 g/L against *E. coli* and *M. flavus*. Bars indicate the absorbance of the bacterial culture (black bars), the culture treated with CS (light gray bars), CSE (red bars), acetic acid (yellow bars), Ag NPs (grey bars), Ag@CSE (silver grey) and Ag@CS (dark grey). Data are expressed as mean ± standard deviation. Different letters indicate significant differences ($p < 0.05$) between absorbance values of the bacterial culture alone and that of bacteria treated with the different concentrations of each treatment (data were analyzed with one-way Anova and Bonferroni *post-hoc* test).

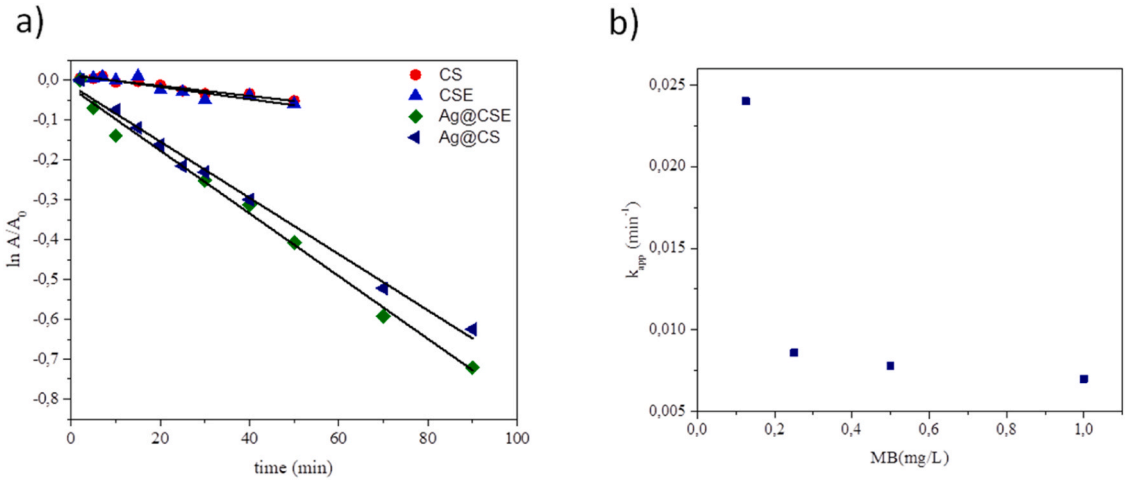

Fig. 7. a) Plots of ln(A/Ao) against time for reduction of MB (1 mg/L) in CS, CSE, Ag@CS and Ag@CSE solutions; b) plot of k(min-1) as a function of MB concentration for the reaction in Ag@CS solution.

and to the accumulation of intermediate products that will reduce the reaction between MB and the active species. Considering the CSE system, the rate constants and efficiency evaluated for CSE and Ag@CSE, were comparable to the same parameters evaluated for the experiments carried out with CS. These results allow to state that the CSE can be used as an economically and ecologically sustainable alternative to commercial chitosan sources in the photodegradation of organic dyes.

Conclusions

In this work, we successfully synthesized silver nanoparticle-chitosan (Ag@CS) composites via nanosecond laser ablation in liquid, employing both commercial chitosan and chitosan extracted from an alternative and sustainable source, i.e. the pupal exuviae of *Hermetia illucens* (Ag@CSE). The comprehensive characterization of the composites, carried out with spectroscopic and microscopic techniques,

confirmed the formation of stable, well-dispersed nanoparticles, and preservation of the chitosan's functional groups throughout the synthesis process. Both Ag@CS and Ag@CSE composites exhibited significant antibacterial activity against *Escherichia coli* and *Micrococcus flavus*, with Ag@CSE outperforming commercial chitosan composites in several tests, especially at lower concentrations. Furthermore, both composites demonstrated efficient photocatalytic degradation of methylene blue, validating their potential in environmental applications. These findings highlight the versatility and effectiveness of laser ablation in producing bio-nanocomposites with multifunctional properties and the promising potential of insect-derived chitosan as a sustainable and high-performance alternative to traditional sources. By validating the functional properties of Ag@CSE, this study advances the field of green nanotechnology and supports the development of eco-friendly materials for biomedical and environmental applications. Future research will focus on integrating these nanocomposites into solid-state membranes, in order to assess their potential use in medical devices and wastewater treatment. Ultimately, the successful exploitation of bioconverter insect waste for advanced nanomaterial production opens new avenues for circular economy strategies and resource-efficient innovation.

CRediT authorship contribution statement

M.M., A.G., M.T., M.C., A.G.,: investigation, data curation, writing, review and editing; C.S., R.S., P.F.: methodology, validation, writing, review and editing, R.T., A. D.B.: conceptualization, methodology, validation, funding acquisition, writing, review and editing

Declaration of Competing Interest

The authors declare that they have no known competing financial interests or personal relationships that could have appeared to influence the work reported in this paper.

Acknowledgment

M.M, A.D. and R.T. acknowledge financial support under the National Recovery and Resilience Plan (NRRP), Mission 4, Component 2, Investment 1.1, Call for tender No. 1409 published on 14.9.2022 by the Italian Ministry of University and Research (MUR), funded by the European Union – NextGenerationEU– Project Title "A Collaborative Multinanozime platform for cancer" (CoMu4CaT)- CUP: C53D23007870001. Grant Assignment Decree No. 1384 adopted on 01/09/2023 by the Italian Ministry of Ministry of University and Research (MUR).

Appendix A. Supporting information

Supplementary data associated with this article can be found in the online version at doi:10.1016/j.nxmate.2025.100952.

Data availability statement

All data are available upon request.

References

[1] R. Álvarez-Chimal, J.A. Arenas-Alatorre, M.A. Álvarez-Pérez, Nanoparticle-polymer composite scaffolds for bone tissue engineering. A review, Eur. Polym. J. 213 (2024) 113093.
[2] P. Karthik, J. Rajesh, S. Ravichandran, Comprehensive review on the advancement of transition metal oxides infused cellulose acetate nanocomposites for the photocatalytic degradation of emerging pollutants, J. Water Process Eng. 66 (2024) 106010.
[3] G. Praveen, S. Rajkhowa, Recent advances of economically synthesised polymers/composites consisting of graphene and silver nanoparticles to achieve sustainable existence, Polym. Bull. 81 (2024) 10461–10487.
[4] A.E. Pérez Mendoza, C. Andronescu, A. Olean-Oliveira, Design of conducting polymer/metal-based nanocomposites as electrocatalysts for electrochemical energy conversion, Synth. Mater. 307 (2024) 117662.
[5] A.A. Manshina, I.I. Tumkin, E.M. Khairullina, M. Mizoshiri, A. Ostendorf, S. A. Kulinich, S. Makarov, A.A. Kuchmizhak, E.L. Gurevich, The second laser revolution in chemistry: emerging laser technologies for precise fabrication of multifunctional nanomaterials and nanostructures, Adv. Funct. Mater. (2024) 2405457.
[6] A. De Bonis, M. Sansone, L. D'Alessio, A. Galasso, A. Santagata, R. Teghil, Dynamics of laser-induced bubble and nanoparticles generation during ultra-short laser ablation of Pd in liquid, J. Phys. D Appl. Phys. 46 (2013) 445301.
[7] A. Khumaeni, T. Istanti, E. Hidayanto, I. Nurhasanah, Characteristics of tin oxide nanoparticles produced by pulsed laser ablation technique in various concentrations of chitosan liquid and their potential application as an antibacterial agent, Results Eng. 16 (2022) 100742.
[8] A.El Askary, N.S. Awwad, H.A. Ibrahium, M.Eid Moustapha, A.A. Menazea, Structural, thermal, morphological and antibacterial activities of hybrid bio-nanocomposite Chitosan/Au/Bi2O3 for biomedical applications, J. Polym. Res. 29 (2022) 269.
[9] A.A. Menazea, M.K. Ahmed, Wound healing activity of Chitosan/Polyvinyl Alcohol embedded by gold nanoparticles prepared by nanosecond laser ablation, J. Mol. Struct. 1217 (2020) 128401.
[10] A.A. Menazea, A.M. Ismail, N.S. Awwad, H.A. Ibrahium, Physical characterization and antibacterial activity of PVA/Chitosan matrix doped by selenium nanoparticles prepared via one-pot laser ablation route, J. Mater. Res. Technol. 9 (2020) 9598.
[11] A.A. Menazea, H.A. Ibrahium, N.S. Awwad, M.Eid Moustapha, M.O. Farea, M. A. Bajaber, Facile synthesis and high-performance dielectric properties of polyethylene oxide-chitosan- iron oxide nano-composite for electrical applications, J. Mater. Res. Technol. 18 (2022) 2273.
[12] M.J. Tommalieh, H.A. Ibrahium, N.S. Awwad, A.A. Menazea, Gold nanoparticles doped Polyvinyl Alcohol/Chitosan blend via laser ablation for electrical conductivity enhancement, J. Mol. Struct. 1221 (2020) 128814.
[13] H. Ali, A.M. Ismail, A.A. Menazea, Multifunctional Ag/ZnO/chitosan ternary bio-nanocomposites synthesized via laser ablation with enhanced optical, antibacterial, and catalytic characteristics, J. Water Process Eng. 49 (2022) 102940.
[14] D.A. Tatarinov, S.R. Sokolnikova, N.A. Myslitskaya, Applying of chitosan-TiO2 nanocomposites for photocatalytic degradation of anthracene and pyrene, J. Biomed. Photon. Eng. 7 (2021) 101301.
[15] A.N. Amitaye, E.E. Elemike, H.B. Akpeji, E. Amitaye, I. Hossain, J.I. Mbonu, A. E. Aziza, Chitosan: A sustainable biobased material for diverse applications, J. Environ. Chem. Eng. 12 (2024) 113208.
[16] R. Ben Aoun, N. Trabelsi, M. Abdallah, I. Mourtzinos, R. Mhamdi, Towards a greener future: exploring the challenges of extraction of chitin and chitosan as bioactive polysaccharides, Mater. Today Commun. 39 (2024) 108761.
[17] M. Triunfo, E. Tafi, A. Guarnieri, R. Salvia, C. Scieuzo, T. Hahn, S. Zibek, A. Gagliardini, L. Panariello, M.B. Coltelli, A. De Bonis, P. Falabella, Characterization of chitin and chitosan derived from Hermetia illucens, a further step in a circular economy process, Sci. Rep. 12 (2022) 6613.
[18] E.A. Ganash, Synthesis of silver nanoparticles using pulsed laser ablation in liquid: a review, Laser Phys. Lett. 20 (2023) 013001.
[19] S.A. Abbasi, J. Javed, H. Qayyum, T.M. Khan, D. Ali, A. Iqbal, S. Aal, N. Nazir, Composite liquid media influence on the optical and bactericidal properties of silver nanoparticles synthesized by pulsed laser ablation in liquids, Plasmonics (2024), https://doi.org/10.1007/s11468-024-02443-w.
[20] M. Marsico, R. Azari, M. Curcio, R. Teghil, M. Triunfo, P. Falabella, A. R. Boccaccini, A. De Bonis, Enhancing the antibacterial properties of chitosan coatings: Ag@ chitosan and chitosan from insects, Coatings 14 (2024) 925.
[21] A.S. Rodrigues, J.G.S. Batista, M.Á.V. Rodrigues, V.C. Thipe, L.A.R. Minarini, P.S. Lopes, A.B. Lugão, Advances in Silver Nanoparticles: A Comprehensive Review on Their Potential as Antimicrobial Agents and Their Mechanisms of Action Elucidated by Proteomics, Frontiers in Microbiology, doi: 10.3389/fmicb.2024.1440065.
[22] A. Guarnieri, M. Triunfo, C. Scieuzo, D. Ianniciello, E. Tafi, T. Hahn, S. Zibek, R. Salvia, A. De Bonis, P. Falabella, Antimicrobial properties of chitosan from different developmental stages of the bioconverter insect Hermetia illucens, Sci. Rep. 12 (2022) 8084.
[23] N.Sh Ashurov, S.M. Yugai, S.Sh Shakhobutdinov, A.S. Kulumbetov, A. A. Atakhanov, Physicochemical studies of the structure of chitosan and chitosan ascorbate nanoparticles, Russ. Chem. Bull. 71 (2022) 227.
[24] M. Saikia, T. Dasa, B.K. Saikia, A novel rapid synthesis of highly stable silver nanoparticle/carbon quantum dot nanocomposites derived from low-grade coal feedstock, N. J. Chem. 46 (2022) 309.
[25] V. Amendola, D. Amans, Y. Ishikawa, N. Koshizaki, S. Scirè, G. Compagnini, S. Reichenberger, S. Barcikowski, Room-temperature laser synthesis in liquid of oxide, metal-oxide core-shells, and doped oxide nanoparticles, Chem. A Eur. J. 26 (2020) 9206.
[26] J. Brugnerotto, J. Lizardi, F.M. Goycoolea, W. Arguelles-Monal, J. DesbrieÁres, M. Rinaudo, An infrared investigation in relation with chitin and chitosan characterization, Polymer 42 (2001) 3569.

[27] S.M. Nasef, H.E. Mohamed, S.Z. Mansour, Effect of Chitosan-silver nanoparticles on DEN-induced hepatocellular injury by regulation of Wnt/β-catenin and apoptosis signaling patways in rats, Chem. Select 9 (2024) e202400356.
[28] M. Triunfo, A. Guarnieri, D. Ianniciello, M.B. Coltelli, R. Salvia, C. Scieuzo, A. De Bonis, P. Falabella, A comprehensive characterization of Hermetia illucens derived chitosan produced through homogeneous deacetylation, Int. J. Biol. Macromol. 271 (2024) 132669.
[29] X. Feng, X. Li, B. Su, J. Ma, Solid-phase fabrication of TiO2/Chitosan-biochar composites with superior UV–vis light driven photocatalytic degradation performance, Colloid. Surf. A 648 (2022) 129114.